Nano World Journal

https://doi.org/10.17756/nwj.2024-s1-045

Research Article

Open Access

Study on the Mechanical Behavior of Aramid Epoxy Composites with Coal Ash Filler

S. Seenivasan[1*], D.F. Melvin Jose[2], R.J. Golden Renjith Nimal[3], S. Madhava Reddy[4], M. Maniyarasan[5], S. Balasubramani[6] and R. Girimurugan[7]

[1]*Department of Mechanical Engineering, Rathinam Technical Campus, Coimbatore, Tamil Nadu, India*
[2]*Department of Mechanical Engineering, AL AZAR College of Engineering and Technology, Thodupuzha, Kerala, India*
[3]*Department of Mechanical Engineering, Jai Shriram Engineering College, Tirupur, Tamil Nadu, India*
[4]*Department of Mechanical Engineering, Mahatma Gandhi Institute of Technology, Hyderabad, Telangana, India*
[5]*Department of Mechanical Engineering, Kongunadu College of Engineering and Technology, Trichy, Tamil Nadu, India*
[6]*Department of Mechatronics Engineering, Sri Krishna College of Engineering and Technology, Coimbatore, Tamil Nadu, India*
[7]*Department of Mechanical Engineering, Nandha College of Technology, Perundurai, Tamil Nadu, India*

***Correspondence to:**
Seenivasan S
Department of Mechanical Engineering,
Rathinam Technical Campus,
Coimbatore, Tamil Nadu, India.
E-mail: seenikct@gmail.com

Received: January 03, 2024
Accepted: March 15, 2024
Published: March 20, 2024

Citation: Seenivasan S, Jose DFM, Renjith Nimal RJG, Reddy MS, Maniyarasan M, et al. 2024. Study on the Mechanical Behavior of Aramid Epoxy Composites with Coal Ash Filler. *NanoWorld J* 10(S1): S250-S258.

Published by United Scientific Group

Abstract

The current study examines the effects of varying the amount of coal ash (CA) used as a filler in woven aramid epoxy (AE) reinforced composites from 0% to 12% by weight. This includes testing the composites' mechanical, water absorption, and thermal characteristics. Samples were made using a hand lay-up approach, and then their qualities are evaluated using conventional ASTM procedures. Industrial fly ash is produced when pulverized coal is burned in a thermal power station. It is a metal oxide combination that is a contaminant that must be disposed of or used. Therefore, turning an industrial byproduct like CA into a bio-reinforced composite material would be a win-win situation. The tensile strength, flexural strength, inter-laminar shear strength (ILSS), and microhardness of the AE composites are all found to increase when 6 wt.% filler is added. The flexural strength decreases by around 20% and the tensile strength by about 7.5% when compared to non-filler loaded composites when filler is added at a weight of 12 wt.%. Microhardness is decreased by 17.4%, and ILSS is decreased to 19.5%. CA filler has a negative effect on impact strength. CA filler added to aramid fiber decreases the composites' heat conductivity and water absorption.

Keywords

Aramid, Epoxy, Coal ash, Mechanical characteristics, Thermal conduction, Water absorptivity

Introduction

Natural fibers' eco-friendliness and mechanical strength have made them a popular choice for many different uses [1]. Their availability is very context- and competition-dependent. For a composite material system to be economically viable, the raw materials used, and manufacturing method must be carefully considered [2]. Natural fiber reinforced composites have been the subject of much research by scientists' keen to find cost-effective solutions [3]. Even with optimal matrix interaction, natural composites are weaker than those reinforced with synthetic fibers [4]. However, their lighter weight and cheaper price make them a practical alternative to glass fiber reinforced composite [5].

To improve mechanical and other qualities, hybridization in the composite

material system is a new approach. Matrix, reinforcement, and a supplemental strengthening like whisker make up a hybrid composite. The composites' characteristics can be further enhanced during this period with additional reinforcing. Using micro- or nano-sized hard spherical fillers improves the composite's surface superiority and toughness. These expensive, stiff sphere fillers are often made of clay or metal [6]. However, CA found in fly ash may be useful for the reasons. It is a cost-effective solution due to its fundamental alumina-silicate hollow micro-spherical form and status as industrial waste [7]. Owing to its fine diffusion, homogeneous, inert, and chemical stabilization, CA is now commonly employed as a filler in polymer matrix composite. The rationale behind incorporating CA into a polymer matrix is [8]: (a) Lessening the need for matrix material, (b) Composites with enhanced characteristics, and (c) Reducing the composites' price.

Aerogel and cenosphere are used to create a lightweight cementitious composite [9]. The material provides high levels of thermal insulation and specific strength. Composites of low or intermediate density have been discovered using CA as filler up to 60% volume by authors [10, 11]. Researchers [12] examined the tribological properties of fly ash after it was incorporated into AF strengthened phenolic composites. Authors [13] observed that adding CA to ceramic/phenolic composites changed their thermal behavior. CA is added to the ceramic/phenolic composite to make it more resistant to ablation [14-16]. When high density polyethylene was mixed with CA and multi-walled carbon nanotubes, the material's mechanical properties improved [17]. While CA has been studied in relation to its application in polymer matrix composites, nothing is known about its effect on natural fiber reinforced composites [18, 19].

As such, the objective of this analysis is to learn what happens when CA is mixed with aramid fibers at varied percentages [20]. CA was chosen not only because of its potential to be blended with fiber reinforced composite, but also because of the disposal challenge it poses. Aramid is easily accessible and inexpensive [21, 22]. This natural fiber is unique even among lignocellulosic fibers since its strength and modulus surpass those of plastic [23]. Polymer matrix composites with aramid have been investigated by scientists [24]. When compared to other composites on the market, it holds its own. Tribological experiments conducted by authors [25] show that AE composites have superior erosion wear behavior than glass-epoxy composites. Epoxy and polyester have been compared by researchers [26] as matrix materials for making aramid-reinforced polymer composites. Epoxy-resin-prepared aramid composites reportedly outperformed polyester-based ones. In addition to describing the existing composite system, this research examines it considering alternative systems utilizing various natural fibers and glass fibers.

Experimentation

The following is a breakdown of the individual components of the AE composites utilized in this investigation, both with and without the use of CA as a filler.

Materials

Aramid material

Aramid is a long, durable fiber that is gathered in the area as a bidirectional roving mat (plain weave) with a yarn count of 95 tex [27]. Dust particles that might prevent proper fiber-matrix adhesion during manufacturing are cleaned from the collected aramid fibers. The next step is to let it out in the sun for three to four days. This study employs an aramid fiber with a low density (1.5 gm/cc) that allows for a lot of freedom in experimentation.

Matrix

The matrix system includes a triethylene tetra-Amine hardener that cures at room temperature and a diglycidyl ether of bisphenol A epoxy resin of the L12 grade.

CA

When combined with epoxy resin, CA causes a highly uniform dispersion and incorporation. CA particles with a high ceramic content have been shown to be chemically permanent, inert, stable, and homogeneous [28]. The density of CA is between 0.5 and 0.8 gm/cc, and its particle size ranges from 60 to 90 microns. It has a slick, greyish white appearance. It has a melting point between 1300 and 1500 °C and is insoluble in water. SiO_2, Al_2O_3, and Fe_2O_3 are its primary ingredients [29].

Fabrication process

The composite consists of an epoxy matrix with aramid fibers and CA filler. The epoxy resin (L12) and hardener (K6) for curing at low temperatures are combined at a ratio of 10:1. The composite is made using a standard hand lay-up method with a 250 mm x 10 mm x 6 mm hardwood mold at room temperature. Two-, three-, four-, and five-layer mats of aramid fiber are used to strengthen epoxy resin in a series of composite specimens. Based on their lamina count, these composites are categorized as 2AE, 3AE, 4AE, or 5AE. The best mechanically performing AE composite was modified by adding CA filler at weight percentages of 0%, 6%, and 12%. The percentages of CA-AE in these filler-loaded composites are 0, 6 and 12%. After curing in the mold for 24 h at room temperature, the composites are ready to be removed. To facilitate the removal of composites from molds, Teflon sheet and silicon spray are utilized. Finally, after 24 h in air, the samples are released from the mold. The composite samples are then sized appropriately for the tests to be performed. Table 1 shows the different designations given to the specimens based on the number of aramid layers and the weight percent of CA used in their preparation. Composite densities are shown alongside the percentages of AE and CA filler used to create them. Density is a useful metric for judging the quality of composites, the characteristics of which vary depending on the mix of matrix and reinforcement components. Using the following equations [30], one may determine the densities of a fiber-strengthened composites.

For single reinforcement composite:

$$\rho_{ct} = \frac{1}{\frac{W_f}{\rho_f} + \frac{W_m}{\rho_m}} \quad (1)$$

Table 1: Experimental arrangement of various specimens.

Symbol	Percentage volume of fiber (%)	Percentage volume of matrix (%)	Percentage volume of filler (%)	Theoretical density (gm/cc)	Experimental density (gm/cc)	Percentage volume of void (%)
Adding of aramid fiber						
2 AE	20	80	0	1.317	1.236	1.14
3 AE	30	70	0	1.275	1.252	1.13
4 AE	40	60	0	1.296	1.284	1.11
5 AE	50	50	0	1.342	1.332	1.15
Adding of CA filler						
0% CA-4 AE	35	65	0	1.289	1.269	1.08
6% CA-4 AE	35	59	6	1.225	1.212	1.07
12% CA-4 AE	35	53	12	1.165	1.152	1.11

For multiple reinforcement and/or filler composite:

$$\rho_{ct} = \frac{1}{\frac{W_{f1}}{\rho_{f1}} + \frac{W_{f2}}{\rho_{f2}} + \ldots + \frac{W_{fn}}{\rho_{fn}} + \frac{W_m}{\rho_m}} \quad (2)$$

Where 'w_f' is fiber weight fraction, 'w_m' is matrix weight fraction, 'ρ_{ct}' is composite density, 'ρ_f' is fiber density, and 'ρ_m' is matrix density.

The formula for determining the void fraction of a composite is [31]:

$$\text{Void fraction} = \frac{\rho_{ct} - \rho_{ex}}{\rho_{ct}} \text{ x } 100 \quad (3)$$

Where 'ρ_{ct}' is theoretical density and 'ρ_{ex}' is experimental density.

Mechanical testing

Tensile testing

The INSTRON -3369 UTM from the 2580 series is used to conduct the tensile test; it is equipped with static load cells that can withstand up to 50 kN. The ASTM 3039 standard calls for testing a 250 mm long by 25.4 mm wide rectangular cross-section sample. For tensile testing, a tab length of 25.4 mm and a speed of 3 mm/min are maintained. Prior to testing, the specimens undergo a thorough visual inspection to detect any flaws in their outer layers. In this test, a single axial force is given to the specimen from both ends. The specimens are held in a device that is screw mounted by moveable and fixed fixtures. Tensile test means are presented for a total of five specimens for each composite type (1AE, 2AE, 3AE, 4AE, 6% CA-4AE, and 12% CA-4AE). Figure 1 depicts the tensile test specimen.

ILSS and flexural strength testing

The 3 points bending test is performed in accordance with ASTM 790, with the flexural and ILSS measurements taken with the same UTM. Each kind of composites is represented by five sets of specimens, each measuring 130 mm by 25.4 mm. A constant 100 mm span and 3 mm/min crosshead speed are maintained. Figure 2 depicts the ideal specimen setup for the flexural test.

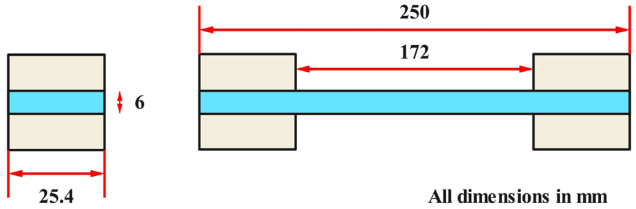

Figure 1: Tensile test sample.

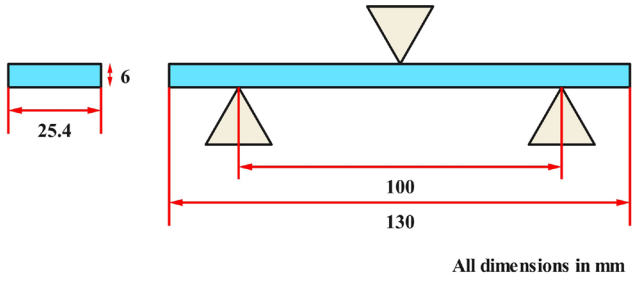

Figure 2: Specimen for the flexural test.

Microhardness testing

Microhardness tests are performed using the Zwick/Roell microhardness tester. The composite sample is indented for 10 sec at a force of 1 kg using a diamond indenter (a right pyramid with a square base and an angle of 136° between opposing sides). The Vickers hardness scale may be read directly from the screen. The average evaluation findings for each composite are shown after testing five individual samples.

Impact strength testing

ASTM D 256 specifies the size and shape of the impact test specimens at 65 mm by 12.7 mm. The 'V' notch is cut at the prescribed 2.0 mm depth and 45° angle. The specimens are broken in an impact testing machine. The amount of energy that was absorbed by the samples during their breakage is recorded.

Water absorption testing

Composites are tested for their ability to absorb water using a method specified in ASTM D 570-98. Cut to 70 mm span and 12.7 width, these samples represent a range of filler

and fiber loadings. Before submerging the sample in distilled water, its original mass is recorded. The samples are submerged in water, then removed and dried on tissue paper. An analytical balance capable of extreme precision is used to weigh the samples. This procedure is continued at 24-h intervals until a steady state is reached. The percentage of moisture in the sample may be determined with the help of equation 4.

$$M_t = \frac{(w_t - w_0)}{w_0} \text{ x } 100 \quad (4)$$

Where 'M_t' is percentage of moisture gain, 'w_0' is pre-aging mass of the specimen, and 'w_t' is variations in the mass of the specimen as it absorbs moisture over time.

Thermal conduction test

The thermal conduction of a non-conductive substance may be measured with Lee's disc equipment. The composite sample is held between two copper discs, each with a diameter of 50 mm and a thickness of 10 mm, which are put above the induction heater. A consistent temperature is achieved by use of a heat source. Two copper discs' temperatures are monitored using thermocouples. Equation 5 can be used to determine the composite sample's thermal conductivity, denoted by the letter k.

$$k = \frac{mC\left(\frac{dT}{dt}\right)_{T_2} \text{ x } d}{A(T_1 - T_2)} \quad (5)$$

Where 'T_1' is temperatures of copper disc 1, 'T_2' is temperatures of copper disc 2, and 'T_1 - T_2' is temperature variation across the composite specimen.

Composite specimens' area (A) and thickness (d) are used here. At a constant temperature, the rate at which a metallic disc radiates heat into its environment is:

$$Q = mC\left(\frac{dT}{dt}\right)_{T_2} \quad (6)$$

A copper disc at temperature T_2 has a mass of m, a heat capacity of C, and a rate of cooling of dT/dt. The theoretical model is also employed to evaluate the thermal conductivity of these composite. The contrary rules of mixing (ROM), as assumed by equation 7, can be used to forecast the effective thermal conductivity of filler particles in matrix.

$$\frac{1}{k_m^{'}} = \frac{v_p}{k_p} + \frac{(1 - v_p)}{k_m} \quad (7)$$

The thermal conduction (k) and the percentage volume of fiber (v_f), are represented in equation 8. The particles of filler and the matrix are denoted by p and m, respectively, in equation 8. The equaiton 8 may be used to roughly estimate the thermal conductivity (k) of fiber-reinforced composites including filler particles scattered throughout the matrix.

$$\frac{1}{k} = \frac{v_f}{k_p} + \frac{(1 - v_f)}{k_m^{'}} \quad (8)$$

Results and Discussion

Tensile strength

Figure 3, shows the tensile strength of an AE composite improves as the number of fiber layers grows from 2 to 3 and finally to 4. The aramid fiber in an AE composite is the material's primary structural component. The tensile strength of a composite material benefits from an enhancement in the weight fraction of fibers. However, the tensile load is reduced when the material is fabricated using a five-layer aramid with fiber epoxy. The tensile strength may have dropped because the aramid fiber wasn't properly and thoroughly impregnated. It's possible that poor adhesion between the aramid and epoxy matrix was brought on by a paucity of matrix material.

When compared to the other composites, the one made by weaving four layers of aramid fiber into an epoxy matrix had the highest tensile strength [10]. Therefore, this 4-layer composite (4AE) is tested for its tensile properties by using filler material comprised of 5 wt.% and 10 wt.% CA. As can be observed in figure 4, the tensile strength of AE composites was increased by around 43% when CA particles were used as filler. The inclusion of 5 wt.% CA explains the improvement because of the enhanced stress transfer from the matrix phase to the aramid material. The tensile strength of an aramid fiber reinforced polymer composite is increased by 45% when 3 wt.% of montmorillonite nanofiller is added [32]. Compared to a pure high density polyethylene matrix, the Young's modulus of oil palm fiber reinforced composites increased by 49% at a nanofiller loading of 12.5 wt.%. CA's use in composites boosts their tensile strength, suggesting increased fiber-matrix adhesion.

Increased strength is the result of better adhesion between the matrix and the fibers. When CA is added to AZ91D magnesium alloy, similar results are found: the composites with 6 wt.% CA have the best compressive strength, while the composites with 12 wt.% CA have the highest compressive yield strength. Consequently, the tensile strength of the composite is found to be almost 7.5% lower when 10% CA is added compared to when no filler is used. CA in this proportion may have impeded appropriate filler dispersion in the composite, leading to the occurrence of local phase inversion. Fiber pull-out and fiber breakage are both evident in the illustration. This demonstrates the mechanical connection and interaction among the fiber and epoxy composites.

Flexural strength and ILSS

As shown in figure 5, epoxy composites reinforced with four layers of aramid fiber perform exceptionally well under severe flexure. The composites' weight proportion of aramid fiber improves their capacity to absorb flexural peak load. Flexural strength drops drastically when epoxy isn't properly impregnated into a 5-layer composite.

Figure 6 indicates how the flexural strength of AE composites changes when CA is added. Increasing the percentage of CA filler from 0 to 6 wt.% results in a significant improvement of about 22%. Possible explanations for this rise include

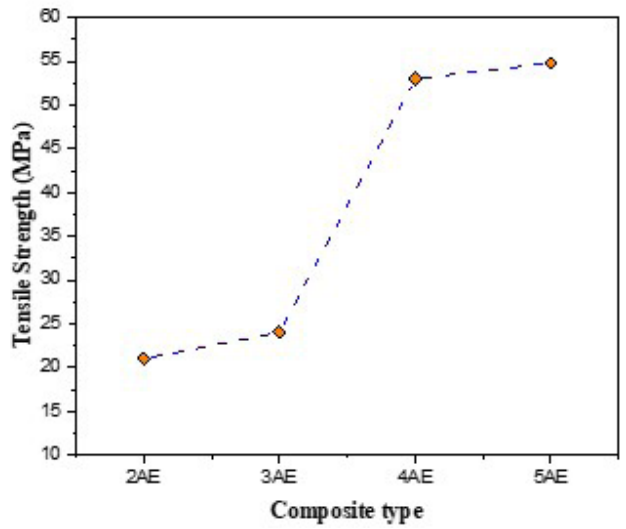

Figure 3: Composites' tensile strength changes with fiber loading.

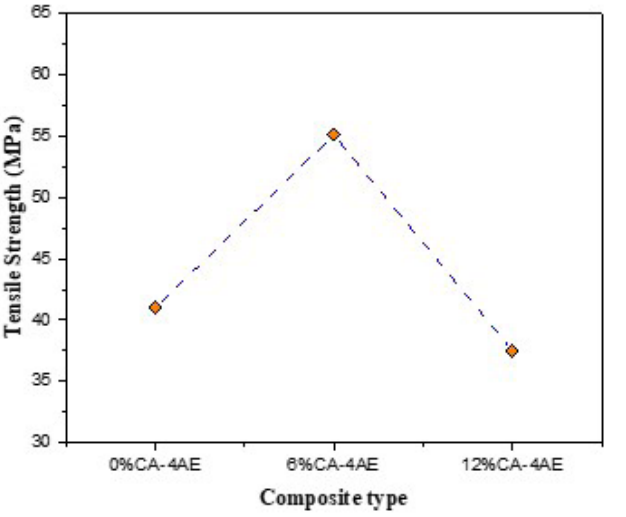

Figure 4: Composites' tensile strength as a function of filler loading.

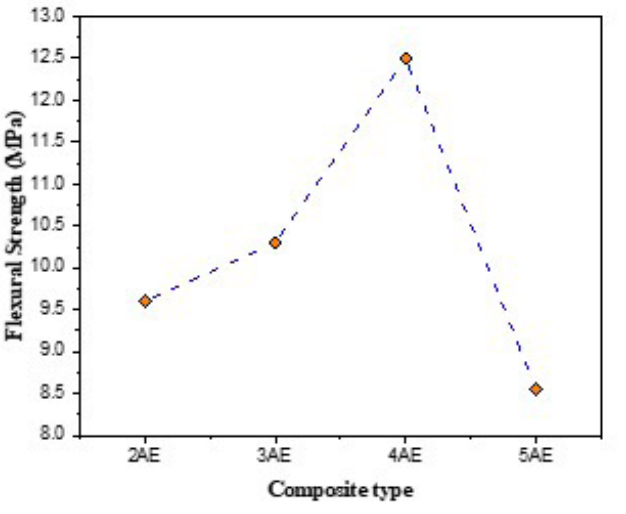

Figure 5: Composite flexural strength as a function of fiber loading.

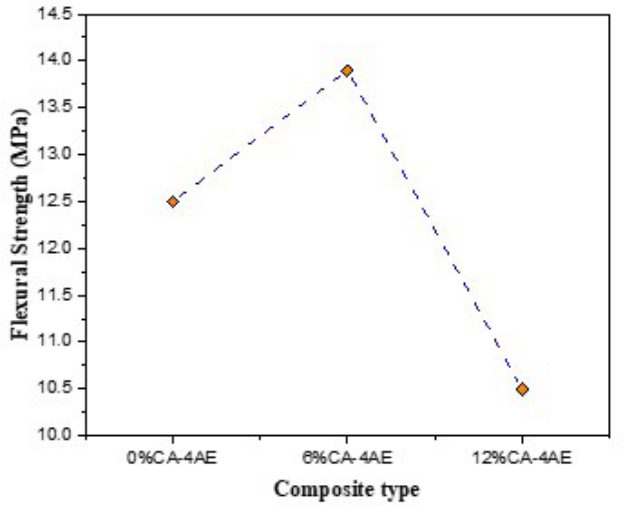

Figure 6: The effect of filler loading on the flexural strength of composites.

developments in adhesion property between epoxy and aramid fiber and enhanced stress transmission from matrix phase to fiber reinforcement. The flexural strength of a composite with no filler decreases by around 20% below 10 wt.% CA due to agglomeration and poor dispersion. Calcium carbonate nanofiller concentrations beyond 4 wt.% in epoxy show a similar trend. The best flexural strength and the largest increase in percentage are both seen when adding nanofiller at 4 wt.%.

Figure 7 and figure 8 show the ILSS with different fiber and filler loadings. Shear strength has similarities to both tensile and flexural strength. The ILSS grows larger when the aramid weight fraction grows larger. The same pattern is seen when CA is used as a filler, with the ILSS performing better at 6 wt.%. The ILSS of a composite loaded with 6 wt.% of filler is 22% higher than that of a composite loaded with 0 wt.% of filler in a four-layer AE structure.

Microhardness

Figure 9 shows that the toughness of the AE composite rises with the fiber weight percentage (and hence the number of aramid layers). The above graph demonstrates how an increase in the fiber weight percentage of an AE composite leads to improvements in both the surface hardness and the internal structural mechanical characteristics.

Vicker's hardness number of a 4-layer AE composite is shown to be affected by the addition of 6 wt.% and 12 wt.% of CA filler material in figure 10. From 0 to 6 wt.% CA loading, the Vicker's hardness number of a 4-layer AE composite increases by a considerable yet small 4%. CA's presence in the matrix, its comparatively high particle strength, and its greater inhibition of localized matrix deformation during indentation are all possible explanations for this phenomenon. But when filler at 12 wt.% is added, the no filler loading composite suddenly weakens by 17%. It is possible that the inefficient distribution of CA in the 12 wt.% filler filled composite contributed to the precipitous drop in hardness. CA agglomeration in the composite material may have caused a local phase inversion, leading to the incorrect dispersion.

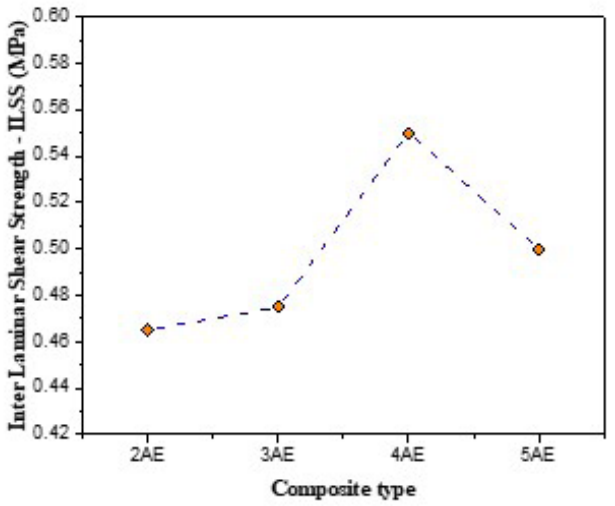

Figure 7: Composites with different fiber loads and their ILSS.

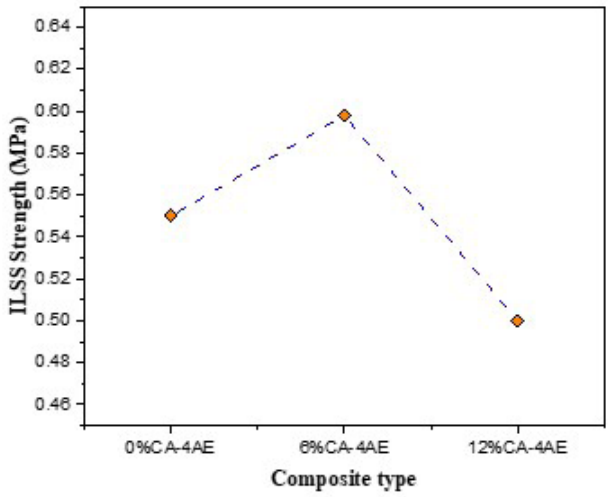

Figure 8: ILSS of composites with different percentage of filler.

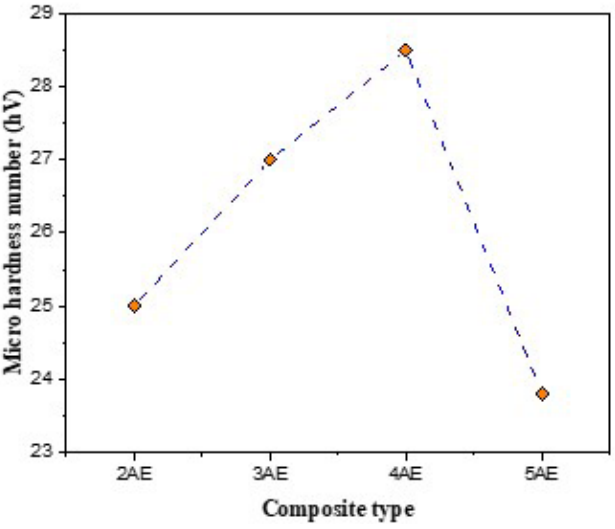

Figure 9: Composite microhardness with variable fiber loading.

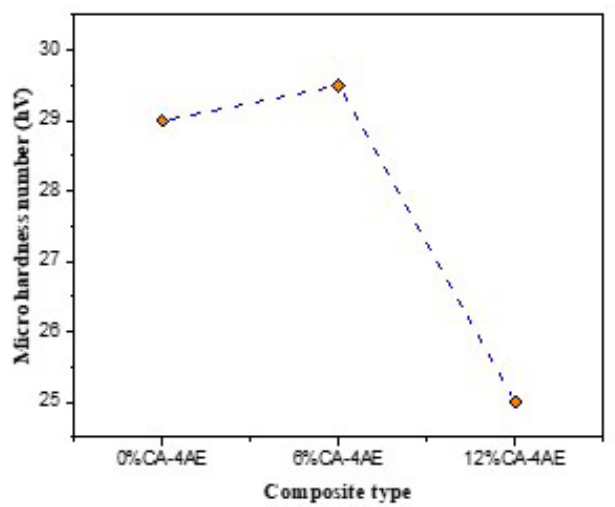

Figure 10: Composite microhardness with respect to filler loading.

Impact strength

Impact resistance of AE composites with varying wt.% of aramid and CA filler loading is shown in figure 11 and figure 12. The maximum value of impact strength is 10.53 KJ/m^2 for a four-layer aramid composite (35 wt.% of fiber). CA filler reduces the kinetic energy of an impact on AE composites. Composites with a filler loading of 12 wt.% have the worst impact strength, while those with no filler loading have the strongest. Impact strength drops by 22% between 0% and 6% moisture content, and by 42% between 0% and 12% moisture content. According to the authors [33], when more CA filler is included into the polymer, the crystallinity of the material suffers. The improved amorphous content has a negative effect on impact toughness.

Water absorption behavior

The proportion of moisture absorbed by different composite samples as a function of immersion time is depicted in figure 13 and figure 14. The moisture absorption curvature shows that the sample absorbs more water as its immersion period rises, up to a saturation point. The rate of absorption has slowed down here. As the percentage of fiber in the composite grows, so does its ability to absorb water. Aramid may have a higher water absorption rate because material contains cellulose, which is a very good moisture absorber. Studies on the water-absorbing capacity of composites made from natural fibers have yielded similar results [34]. Composites lose 18% and 38% of their water-absorbing capacity when filler of 6 wt.% and 12 wt.% is added.

Thermal conductivity

As can be seen in figure 15, the heat conductivity of AE composites decreases as the weight percent of fiber increases. As can be seen in the image, the aramid percentage plays a significant role in determining the heat conductivity of the AE composites. This proves that compared to an epoxy matrix, aramid has better heat conductivity. Figure 16 displays the composites' thermal conductivities as measured experimental-

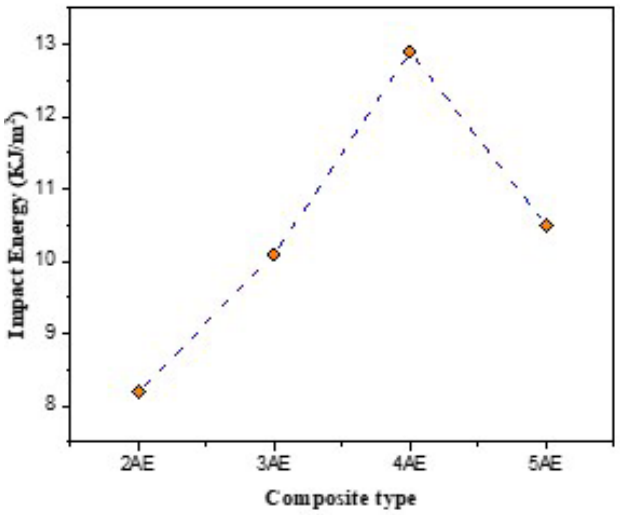

Figure 11: The effect of fiber loading on the impact strength of composites.

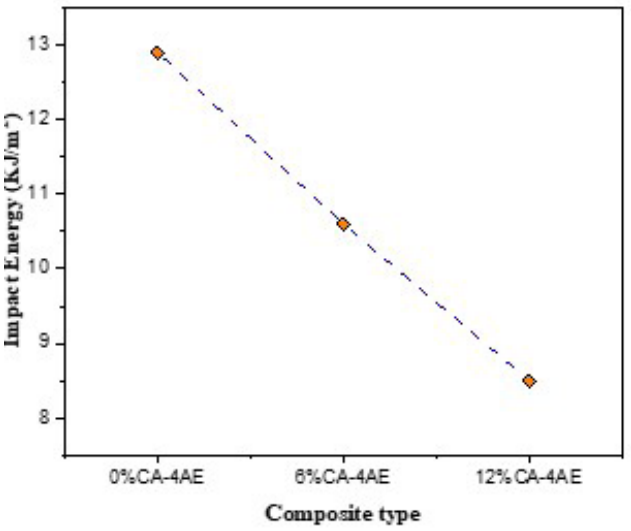

Figure 12: The effect of filler loading on the impact strength of composites.

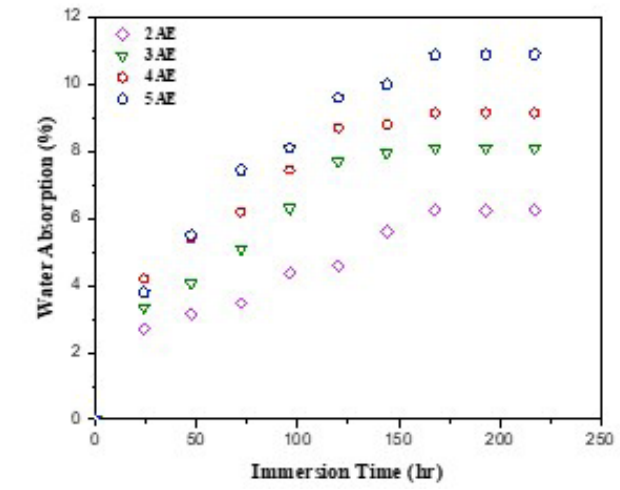

Figure 13: The effect of fiber loading on the composite's water absorption characteristics.

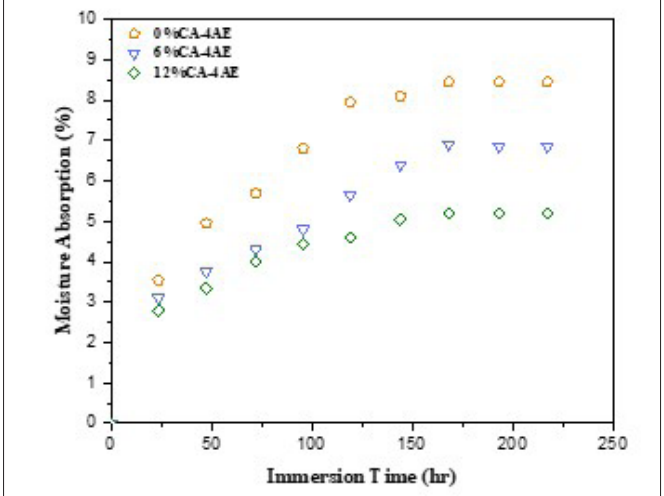

Figure 14: The effect of filler loading on the composite's water absorption behavior.

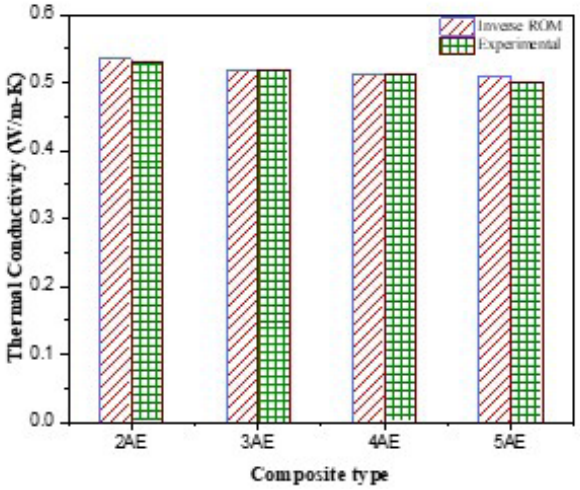

Figure 15: The effect of fiber loading on the thermal conductivity of composites.

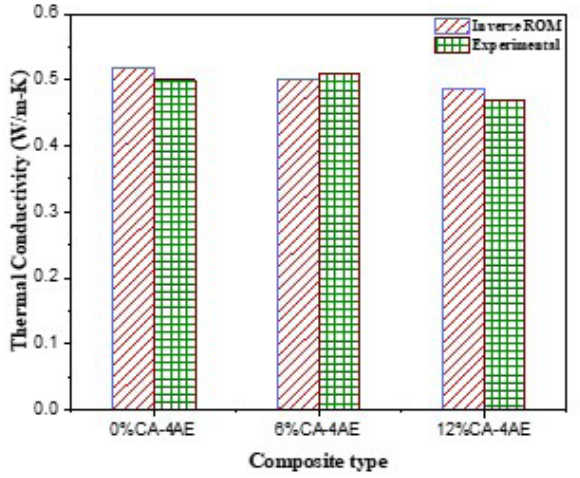

Figure 16: Composites' thermal conductivity as a function of filler loading.

ly and as predicted by the inverse ROM model. Inaccuracies in ROM values range from -1.1% to 0.2% when compared to the experimental value. Because cellulose fiber does not transfer heat, the thermal conductivity of composites reinforced with aramid fiber dropped as the fiber weight percentage increased. This quality has also been found in composites made from banana and sansevieria fiber. CA filler incorporated into an AE matrix increases the heat conductivity of composites, as seen in figure 15. When the filler percentage is increased from 0% to 5%, the thermal conductivity of the matrix drops by around 7.2%. The increase in heat conductivity from 0% to 10% filler is around 9%. Inaccuracies in ROM values range from -1.9% to 1.5% when compared to the experimental value.

Conclusion

Up to around 35 wt.% of fiber may be included into the matrix without compromising the composites' hardness, load-carrying capability (tensile strength), bending resistance (flexural strength), ILSS, or impact strength. The mechanical characteristics of the composites are improved by using up to 6 wt.% of CA in their composition. Filler in composites increases their resistance to water absorption. It grows in proportion to the amount of fiber. As the aramid fiber weight percentage in these composites rises, their thermal conductivity falls. The thermal conductivity of composites made with CA filler is reduced. From no filler to 12% filler, the thermal conductivity changes by around 9%. Values for thermal conductivity calculated using the inverse ROM model compare favorably with those measured experimentally.

This research demonstrates that AE composites may have mechanical qualities that are on par with, or perhaps superior to, glass fiber reinforced composites for certain applications. Aramid fiber composites are weaker than glass fiber reinforced composites, although they are otherwise competitive with the latter in terms of specific and economic qualities due to their low density, biodegradability, and affordability. Due to its improved environmental performance across its whole life cycle and its ability to improve people's economic opportunities, aramid has become more attractive for use in a wide range of contexts.

Acknowledgments

None.

Conflict of Interest

None.

References

1. Mirzaei J, Fereidoon A, Ghasemi-Ghalebahman A. 2022. An investigation into the tensile and impact strength of hybrid nanocomposites reinforced with graphene, kenaf fiber, and basalt fiber. *J Nat Fibers* 19(16): 12896-12910. https://doi.org/10.1080/15440478.2022.2079580
2. Kamath SS, Sampathkumar D, Bennehalli B. 2017. A review on natural areca fibre reinforced polymer composite materials. *Mater Sci Technol* 29(3): 106-128. https://doi.org/10.1016/j.ctmat.2017.10.001
3. Yaghoobi H, Fereidoon A. 2019. Thermal analysis, statistical predicting, and optimization of the flexural properties of natural fiber biocomposites using Box-Behnken experimental design. *J Nat Fibers* 16(7): 987-1005. https://doi.org/10.1080/15440478.2018.1447416
4. Jariwala H, Jain P. 2019. A review on mechanical behavior of natural fiber reinforced polymer composites and its applications. *J Reinf Plast Compos* 38(10): 441-453. https://doi.org/10.1177/0731684419828524
5. Hammiche D, Boukerrou A. 2014. Performances of Composites Based on Alfa Fiber. In Kumar R (ed) Polymer-Matrix Composites: Types, Applications and Performance. Nova Science Publishers, New York.
6. Nayeri MD, Tahir PM, Jawaid M, Harun J, Abdullah LC, et al. 20140. Effect of resin content and pressure on the performance properties of rubberwood-kenaf composite board panel. *Fibers Polym* 15: 1263-1269. https://doi.org/10.1007/s12221-014-1263-z
7. Mirzaei J, Fereidoon A, Ghasemi-Ghalebahman A. 2021. Experimental analysis of mechanical properties of graphene/kenaf/basalt reinforced hybrid nanocomposites using response surface methodology. *J Braz Soc Mech Sci Eng* 43: 215. https://doi.org/10.1007/s40430-021-02936-3
8. Jena I, Kar S. 2021. A Study on Moisture Absorption Test of Alkali-treated Green Fibers. In Acharya SK, Mishra DP (eds) Current Advances in Mechanical Engineering. Lecture Notes in Mechanical Engineering. Springer, Singapore, pp 11-19.
9. Algin Z. 2019. Multivariate performance optimisation of scaffold boards with selected softwood defects. *Constr Build Mater* 220: 667-678. https://doi.org/10.1016/j.conbuildmat.2019.05.190
10. Bagal DK, Parida B, Barua A, Naik B, Jeet S, et al. 2020. Mechanical characterization of hybrid polymer SiC nano composite using hybrid RSM-MOORA-whale optimization algorithm. *IOP Conf Ser Mater Sc Eng* 970(1): 012017. https://doi.org/10.1088/1757-899X/970/1/012017
11. Manral A, Singh R, Ahmad F, Das PP, Chaudhary V, et al. 2023. Multi-objective optimization of mechanical properties of chemically treated bio-based composites using response surface methodology. *Compos Part C Open Access* 10: 100337. https://doi.org/10.1016/j.jcomc.2022.100337
12. Nadondu B, Surin P, Deeying J. 2022. Multi-objective optimization on mechanical properties of glass-carbon and durian skin fiber reinforced poly(lactic acid) hybrid composites using the extreme mixture design response surface methodology. *Case Stud Constr Mater* 17: e01675. https://doi.org/10.1016/j.cscm.2022.e01675
13. Srivabut C, Ratanawilai T, Hiziroglu S. 2022. Response surface optimization and statistical analysis of composites made from calcium carbonate filler-added recycled polypropylene and rubberwood fiber. *J Thermoplast Compos Mater* 35(3): 391-415. https://doi.org/10.1177/0892705719889988
14. Daniyan IA, Mpofu K, Adeodu AO, Adesina O. 2021. Development of carbon fibre reinforced polymer matrix composites and optimization of the process parameters for railcar applications. *Mater Today Proc* 38: 628-634. https://doi.org/10.1016/j.matpr.2020.03.480
15. Tzeng CJ, Yang YK, Hsieh MH, Chen CY. 2011. Adaptive adjustment of injection molding process for mechanical characteristics using the Taguchi method and response surface methodology. *Polym Plast Technol Eng* 50(6): 552-563. https://doi.org/10.1080/03602559.2010.543239
16. Sakin R. 2021. Layup design optimization for e-glass woven roving fabric reinforced polyester composite laminates produced by VARTM. *Fibers Polym* 22(2): 509-527. https://doi.org/10.1007/s12221-021-0087-x
17. Tharazi I, Sulong AB, Mohd Salleh F. 2020. Application of response surface methodology for parameters optimization in hot pressing kenaf reinforced biocomposites. *J Mech Eng* 17(3): 131-144.
18. Thakur RK, Sharma D, Singh KK. 2019. Optimization of surface roughness and delamination factor in end milling of graphene modified GFRP using response surface methodology. *Mater Today Proc* 19: 133-139. https://doi.org/10.1016/j.matpr.2019.06.153
19. de Araujo Alves Lima R, Kawasaki Cavalcanti D, de Souza e Silva Neto J, Meneses da Costa H, Banea MD. 2020. Effect of surface treatments

on interfacial properties of natural intralaminar hybrid composites. *Polym Compos* 41(1): 314-325. https://doi.org/10.1002/pc.25371

20. Bing DU, Liming CH, Houchang LI, Qinghao HE, Weiming QI, et al. 2020. Resistance welding of glass fiber reinforced thermoplastic composite: experimental investigation and process parameter optimization. *Chin J Aeronaut* 33(12): 3469-3478. https://doi.org/10.1016/j.cja.2020.02.018
21. Asma B, Hamdi L, Ali B, Youcef M. 2020. Flexural mechanical properties of natural fibre reinforced polymer composites — a statistical investigation. *Fibers Polym* 21: 2321-2337. https://doi.org/10.1007/s12221-020-1299-1
22. Bhargav KV, Shanthan P, Balaji PS, Sahu RK, Sahoo SK. 2022. Generation of microholes on GFRP composite using ES-μ-ECDM system. *CIRP J Manuf Sci Technol* 38: 695-705. https://doi.org/10.1016/j.cirpj.2022.06.015
23. Zhang Z, Sun W, Zhao Y, Hou S. 2018. Crashworthiness of different composite tubes by experiments and simulations. *Compos Part B Eng* 143: 86-95. https://doi.org/10.1016/j.compositesb.2018.01.021
24. Rajesh S, Bhaskar GB, Subash R, Pazhanivel K, Sagadevan SS. 2017. Optimization of composite leaf spring design using response surface methodology. *Rom J Mater* 47(1): 98-105.
25. Kunnan Singh JS, Ching YC, Abdullah LC, Ching KY, Razali S, et al. 2018. Optimization of mechanical properties for polyoxymethylene/glass fiber/polytetrafluoroethylene composites using response surface methodology. *Polymers* 10(3): 338. https://doi.org/10.3390/polym10030338
26. Jesthi DK, Nayak RK. 2020. Sensitivity analysis of abrasive air-jet machining parameters on machinability of carbon and glass fiber reinforced hybrid composites. *Mater Today Commun* 25: 101624. https://doi.org/10.1016/j.mtcomm.2020.101624
27. Surendran S, Sundaram T, Sathish Kumar P. 2022. Optimization of surface roughness and tool wear during machining of AMMC using taguchi technique. *Chiang Mai J Sci* 49(6): 1653-1662.
28. Satishkumar P, Dharmalingam S, Raja K, Lingadurai K, Padmanaban G. 2015. Investigation on electrochemical micro machining of Al 6061-6% wt Gr based on taguchi design of experiments. *Int J Chem Tech Res* 7(1): 203-211.
29. Jain K, Kumar BS, Gopalan V, Vimalanand S, Ayyappan S. 2018. Vibrational analysis of hybrid fabric-reinforced polymer matrix curved composite beams. *Compos Mech Comput Appl Int J* 9(3): 269-282. https://doi.org/10.1615/CompMechComputApplIntJ.2018020127
30. Dash S, Routara BC, Nayak RK. 2017. Optimization of process parameters in milling of TiO_2 filled GFRP composite. *Mater Today Proc* 4(2): 3023-3032. https://doi.org/10.1016/j.matpr.2017.02.185
31. Satishkumar P, Saravana Murthi C, Chebolu R, Rao YS, Capangpangan RY, et al. 2022. Optimizing the mechanical and microstructure characteristics of stir casting and hot-pressed AA 7075/ZnO/ZrO_2 composites. *Adv Mater Sci Eng* 2022: 6559014. https://doi.org/10.1155/2022/6559014
32. Shah SA, Kahla NB, Atig M, Anwar MK, Azab M, et al. 2023. Optimization of fresh and mechanical properties of sustainable concrete composite containing ARGF and fly ash: an application of response surface methodology. *Constr Build Mater* 362: 129722. https://doi.org/10.1016/j.conbuildmat.2022.129722
33. Abd Razak SI, Sharif NF. 2015. Concurrent optimization of the mechanical and electrical properties of polyaniline modified kenaf paper. *Cellul Chem Technol* 49(2): 195-202.
34. Sepe R, Bollino F, Ceparano A, Lamanna G. 2016. Mechanical properties of hemp fibre/epoxy composites. Influence of fibre chemical treatments. In Proceeding of the 17th European Conference on Composite Materials, Munich, Germany.